ARMY RESEARCH LABORATORY

Influence of Pulse Length on Electrothermal Plasma Jet Impingement Flow

by Lang-Mann Chang and Stephen L. Howard

ARL-TR-4348 **December 2007**

NOTICES

Disclaimers

The findings in this report are not to be construed as an official Department of the Army position unless so designated by other authorized documents.

Citation of manufacturer's or trade names does not constitute an official endorsement or approval of the use thereof.

Destroy this report when it is no longer needed. Do not return it to the originator.

Army Research Laboratory
Aberdeen Proving Ground, MD 21005-5066

ARL-TR-4348 **December 2007**

Influence of Pulse Length on Electrothermal Plasma Jet Impingement Flow

Lang-Mann Chang
American Systems Corporation

Stephen L. Howard
Weapons and Materials Research Directorate, ARL

REPORT DOCUMENTATION PAGE	Form Approved OMB No. 0704-0188

1. REPORT DATE *(DD-MM-YYYY)*	2. REPORT TYPE	3. DATES COVERED (From - To)
December 2007	Final	October 2004–September 2006

4. TITLE AND SUBTITLE
Influence of Pulse Length on Electrothermal Plasma Jet Impingement Flow

5a. CONTRACT NUMBER

5b. GRANT NUMBER

5c. PROGRAM ELEMENT NUMBER

6. AUTHOR(S)
Lang-Mann Chang* and Stephen L. Howard

5d. PROJECT NUMBER
622618.H8000

5e. TASK NUMBER

5f. WORK UNIT NUMBER

7. PERFORMING ORGANIZATION NAME(S) AND ADDRESS(ES)
U.S. Army Research Laboratory
ATTN: AMSRD-ARL-WM-BD
Aberdeen Proving Ground, MD 21005-5066

8. PERFORMING ORGANIZATION REPORT NUMBER
ARL-TR-4348

9. SPONSORING/MONITORING AGENCY NAME(S) AND ADDRESS(ES)

10. SPONSOR/MONITOR'S ACRONYM(S)

11. SPONSOR/MONITOR'S REPORT NUMBER(S)

12. DISTRIBUTION/AVAILABILITY STATEMENT
Approved for public release; distribution is unlimited.

13. SUPPLEMENTARY NOTES
*American Systems Corporation, 13990 Parkeast Circle, Chantilly, VA 20151

14. ABSTRACT
An experimental investigation has been performed to gain insight into the flows resulting from a plasma jet impinging on a flat plate at representative incident angles of 90°, 60°, and 45° in the open air for two plasma pulse lengths (~0.3 and 1.0 ms). Specifically, the investigation examined the influence of the pulse length on the flow characteristics that may affect the plasma-propellant interactions occurring in the electrothermal chemical charge system. Comparisons for the two pulse lengths were made with data including flow pattern, pressure distribution, light intensity, and flow signature on the impingement plate. Distinct differences in these data were observed between the two pulse lengths. Overall results showed that although the plasma with a shorter pulse length was more powerful, it had a shorter time duration of flow interaction. Therefore, the pulse length can be a key parameter to be optimized in order to effectively ignite a charge system with a minimum requirement of electrical energy. Differences in the results from variable incident angles of jet impingement were also evident.

15. SUBJECT TERMS
electrothermal plasma jet impingement flow, pulse length, charge ignition, igniter studies, plasma-propellant interaction

16. SECURITY CLASSIFICATION OF:			17. LIMITATION OF ABSTRACT	18. NUMBER OF PAGES	19a. NAME OF RESPONSIBLE PERSON
a. REPORT	b. ABSTRACT	c. THIS PAGE			Lang-Mann Chang
UNCLASSIFIED	UNCLASSIFIED	UNCLASSIFIED	UL	26	19b. TELEPHONE NUMBER (*Include area code*) 410-278-6692

Standard Form 298 (Rev. 8/98)
Prescribed by ANSI Std. Z39.18

Contents

List of Figures

1. Introduction

The potential benefits of using electrothermal plasma to achieve rapid and reproducible ignition, as well as to compensate the temperature sensitivity of propelling charges, have been recognized for years (*1–4*). In this regard, substantial research activities have been performed on plasma characteristics (*5–9*) and plasma-propellant interactions (*10–23*). Significant progress has been reported in understanding these areas. Furthermore, researchers have conducted both experiments and computer modeling to investigate plasma flows in closed chambers packed with inert or live propellant (*24, 25*). These studies include flow dynamics as present in actual gun charge configurations. However, for this novel propulsion technology to be effective, a fundamental understanding of the jet flow and its controlling parameters needs to be obtained.

Recently, Chang and Howard examined the flow patterns of a plasma jet effused from a capillary into the open air for two pulse lengths of ~0.3 and 1.0 ms (*26*). For the two pulse lengths, profound differences were observed in time duration of jet appearance, flow field width, flow penetration, and light intensity. Other experiments with a 25-mm closed chamber packed with disk propellant in a conceptual configuration also showed a strong effect of the pulse length on the flame propagation in the propellant bed. Most recently, Beyer conducted experiments involving a 30-mm gun (*27*). The results again showed the effect of the pulse length on the charge-system ignition delay.

The present work focuses on the flow dynamics resulting from a plasma jet impinging on a flat plate at variable incident angles (90°, 60°, and 45°) in the open air for the two pulse lengths. Such impingement flows may occur when the plasma jet enters the propellant bed in a charge system. Result comparisons are made for the influence of the pulse length.

2. Experimental

Figure 1 is a photograph of the experimental setup for the present studies, which consists of a plasma generator, a jet impingement plate, and the common mounting plate. The plasma generator is basically an erosive plasma capillary composed of a 9.5-mm outside-diameter and 3.2-mm inside-diameter polyethylene tube housed in a stainless steel cylinder. Inside the polyethylene tube is a 0.1-mm outside-diameter nickel filament, commonly called exploding wire (an element that initiates the plasma flow). This material has been used extensively for capillary components in the past (*2*). The electrodes at the ends of the exploding wire are made of a 3.2-mm tungsten rod at one end (anode) and an expendable steel nozzle, which is threaded

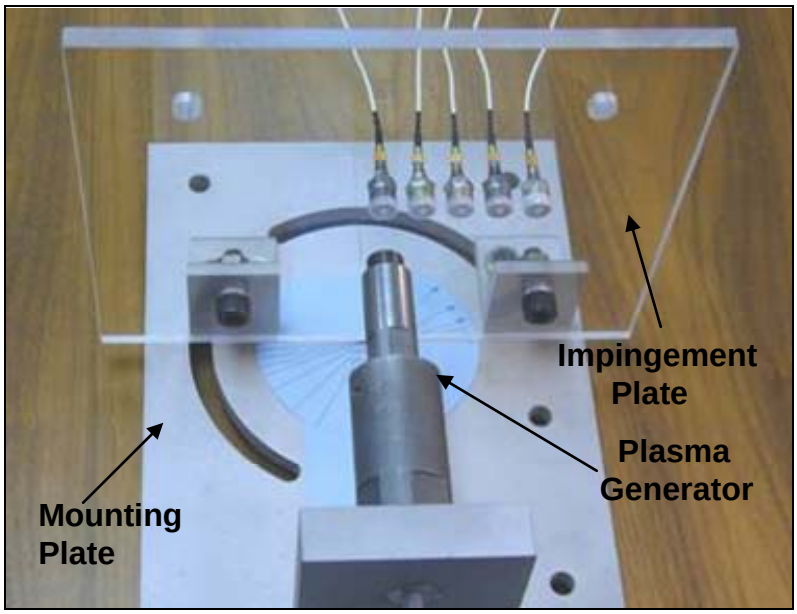

Figure 1. Experimental setup.

into the forward end of the stainless steel cylinder, at the other end (cathode). The nozzle (3.2 mm in diameter) is also used to hold the polyethylene tube in place and to guide the plasma flow to the open space. The effective capillary tube length is adjustable, giving a length-to-diameter ratio of 12 to 22. It has been determined that the ratio of 16 delivers energy efficiently for the present experimental system. The pulsed power supply used is capable of delivering energy up to 3 kJ at a charging level of 3 kV.

The impingement plate is made of a 19-mm thick optically clear acrylic plate. Acrylic is chosen to provide an excellent signature of the jet impingement flow on the plate for photography after firing and to minimize potential interference from the magnetic field created from the plasma on pressure measurements. Figure 2 indicates locations of the pressure ports for pressure-distribution measurement in the radial direction, equally spaced (2 cm) from the center of the impingement area. This center is carefully aligned with the centerline of the nozzle. The distance S is the separation of the impingement plate from the nozzle exit along the centerline. It is set to 25 mm for all tests. The impingement plate can be rotated to give any specific incident angles of the incoming jet flow.

In all experiments, a Phantom V high-speed digital camera was employed for high-speed photography of plasma flow. The camera can record events at a frame rate of up to 64,000 pictures/s. In present studies, a frame rate of 13,000 to 20,000 pictures/s was adequate for capturing details of the flow field. A neutral-density optical filter was placed in front of the camera lens to attenuate the plasma light so that details of the flow structure, especially the shock flow structure, could be better visualized. For pressure measurements, Kistler pressure gages (Model 211B1) were installed behind the impingement plate.

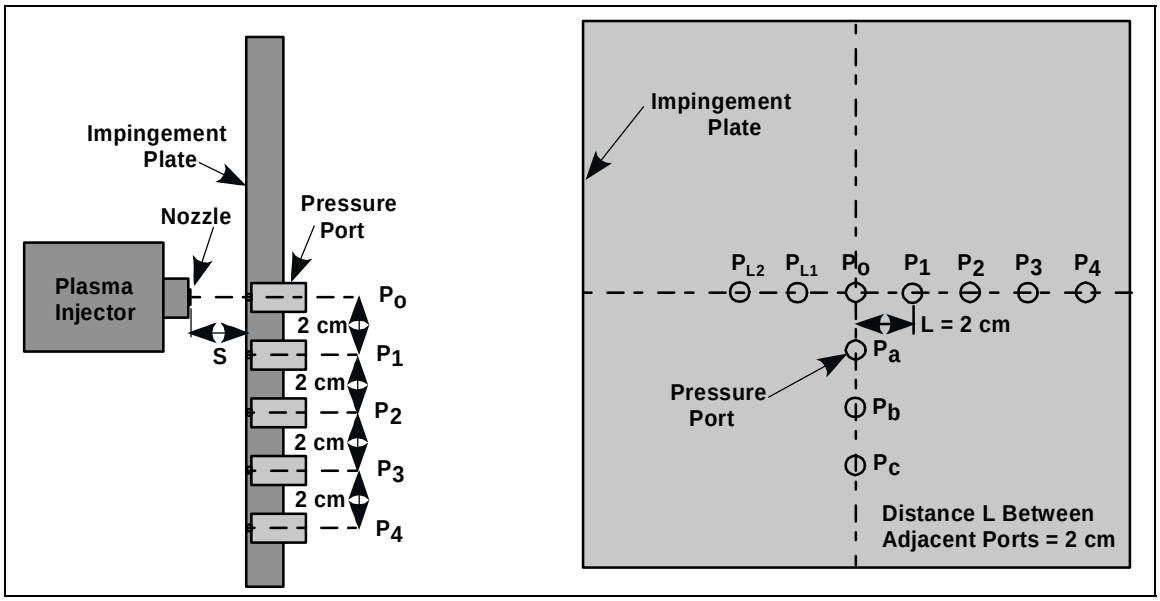

Figure 2. Locations of pressure ports.

The voltage and current through the capillary are recorded using Pearson coils. In turn, these data are used to calculate the power and energy output of the capillary.

3. Results and Discussion

The short pulse length (~0.3 ms) was produced directly from the existing power supply system in the laboratory, while the long one (~1.0 ms) was obtained by adding an inductor to the system. Figure 3 presents typical measurements of the voltage and current, along with calculated power and energy output. Although their resulting energy outputs were at about the same level, the voltage and current were significantly higher for the short pulse system.

Previous visualization studies of a plasma jet flow into still air (see figure 4) revealed the formation of a barrel shock, a normal shock, and a precursor shock in the flow field (*26*). While giving an increased time duration of flow, an increased pulse length resulted in a noticeable reduction of flow field width and light intensity. However, the flow penetration (distance traveled) into still air was greater for a longer pulse length.

After gaining a fundamental understanding of the free plasma jet flow, the present studies show the flow characteristics of plasma jets impinging on a flat plate at variable incident angles of 90°, 60°, and 45°. Results to be presented and compared include the flow pattern, the pressure distribution, and the flow signature on the impingement plate resulting from the short and long pulse lengths.

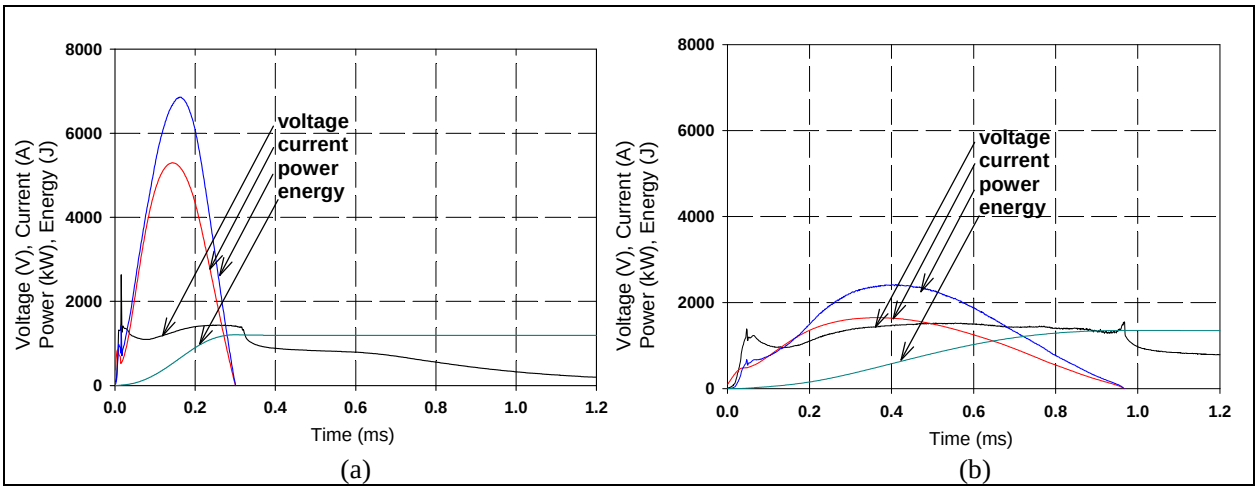

Figure 3. Electrical outputs—voltage, current, power, and energy: (a) short pulse length and (b) long pulse length.

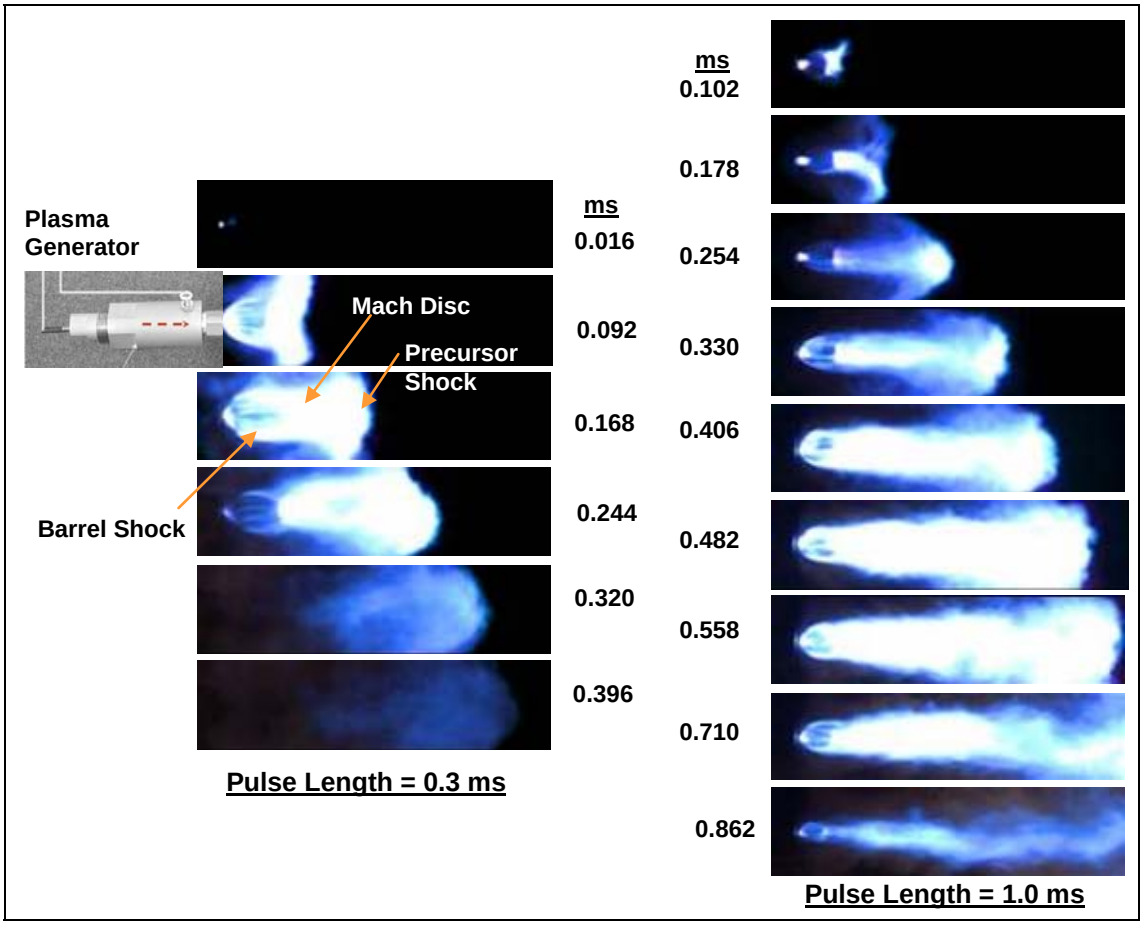

Figure 4. Plasma jet flows in open air.

3.1 Flow Patterns

In the test series with the long pulse length, the camera framing rate and the lens aperture were set at 13,100 frames/s and f/11, respectively. In addition, an optical filter (neutral density index 1.2) was placed in front of the camera. This setup allowed for visualizing the shock wave structure within the flow field. For the short pulse length (since the light intensity and the flow speed were much higher), the previous setup was adjusted to 20,000 frames/s for the framing rate, f/16 for the lens aperture, and neutral density index 2.1 for the optical filter.

3.1.1 The 90° Impingements

Figure 5a exhibits a series of photographs obtained from the high-speed digital camera for the evolution of the flow field for the long pulse length. The first visible light appeared at approximately 0.092 ms after triggering the ignitron. Highly illuminated regions that may represent high-temperature regions can be identified clearly and immediately in front of the nozzle, in the Mach disc, and in the impingement areas. The boundaries of the conical barrel shock are visible. While propagating outward from the stagnation region, the leading part of the flow tended to separate from the impingement plate and curved up gradually, developing into a shape that closely resembles a sombrero. The flow separation was attributed to the large difference in molecular weight between the plasma gas and the ambient air—a classical example of flow instability occurring at the interface of two fluids with different densities in relative motion.

For the short pulse length, a similar flow development is illustrated in figure 5b. However, the light intensity was actually much higher since these images were recorded with a heavier optical filter and a higher lens aperture setting. The width of the flow field was greater, and the flow process took place faster. These flow characteristics are well-correlated to the higher power output indicated in figure 3.

3.1.2 The 60° Impingements

Figure 6a shows the flow-field time histories for the long-pulse plasma jet impinging on the flat plate at the incident angle of 60°. In this test arrangement, flow separation commenced almost from the very beginning, and the leading part of the flow curved up more obviously, developing into the shape of an ocean surge front. Flow turbulence along the flow stream on the plate became increasingly apparent along the upper surface of the flow stream at approximately 0.55 ms and then along the central core of the mainstream at a later period of time. Note that the barrel shock in front of the nozzle remained visible until the last frame of the figure, indicating that the flow there remained supersonic until the end of the electrical pulse.

Figure 6b shows the flow development in time for the short pulse length. As observed in the test with the 90° impingement, the flow evolution proceeded much faster compared with the long pulse length. The flow separation was also more evident. In this case, the distance that the flow traveled on the plate was relatively shorter.

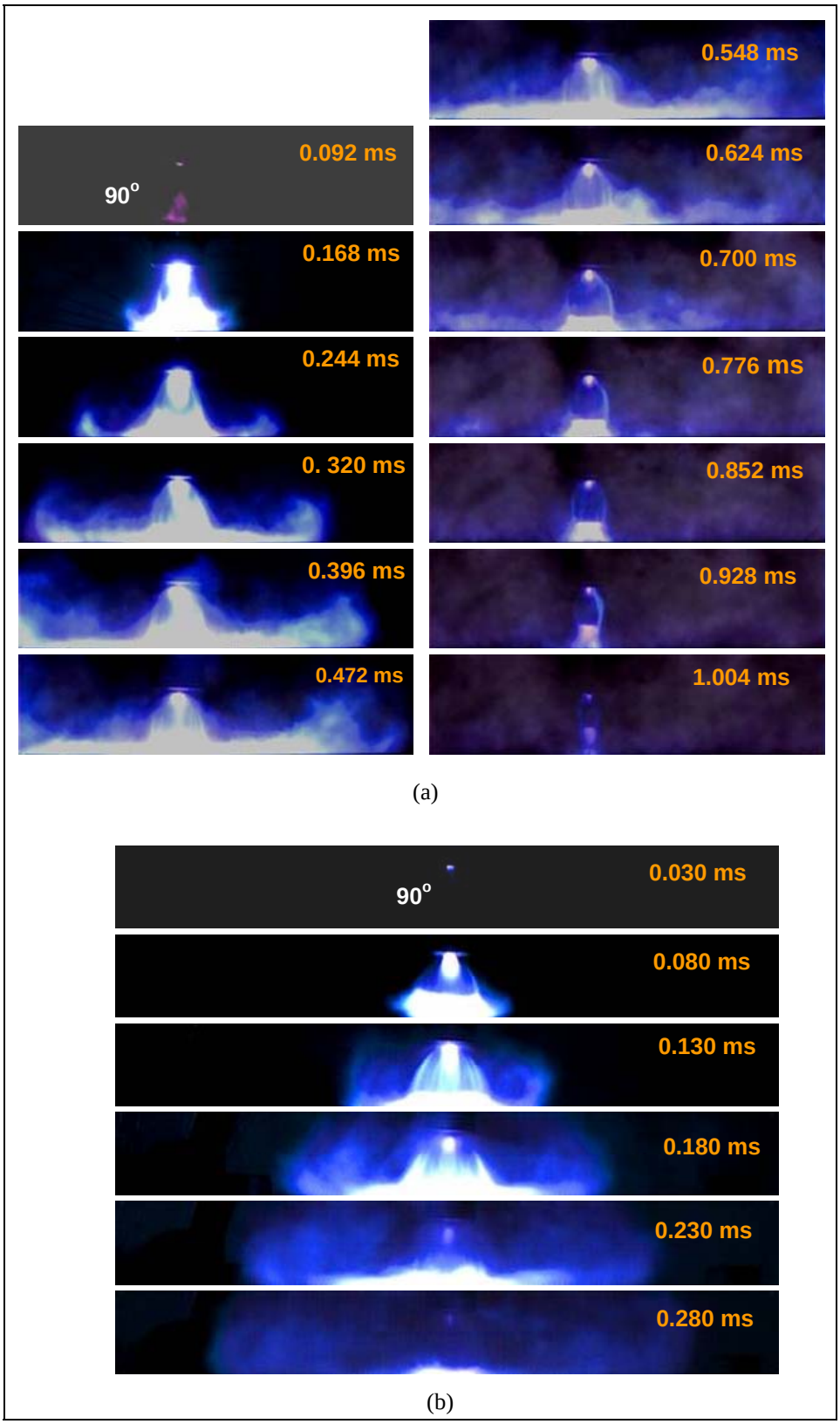

Figure 5. The 90° plasma jet impingement flows: (a) long pulse length and (b) short pulse length.

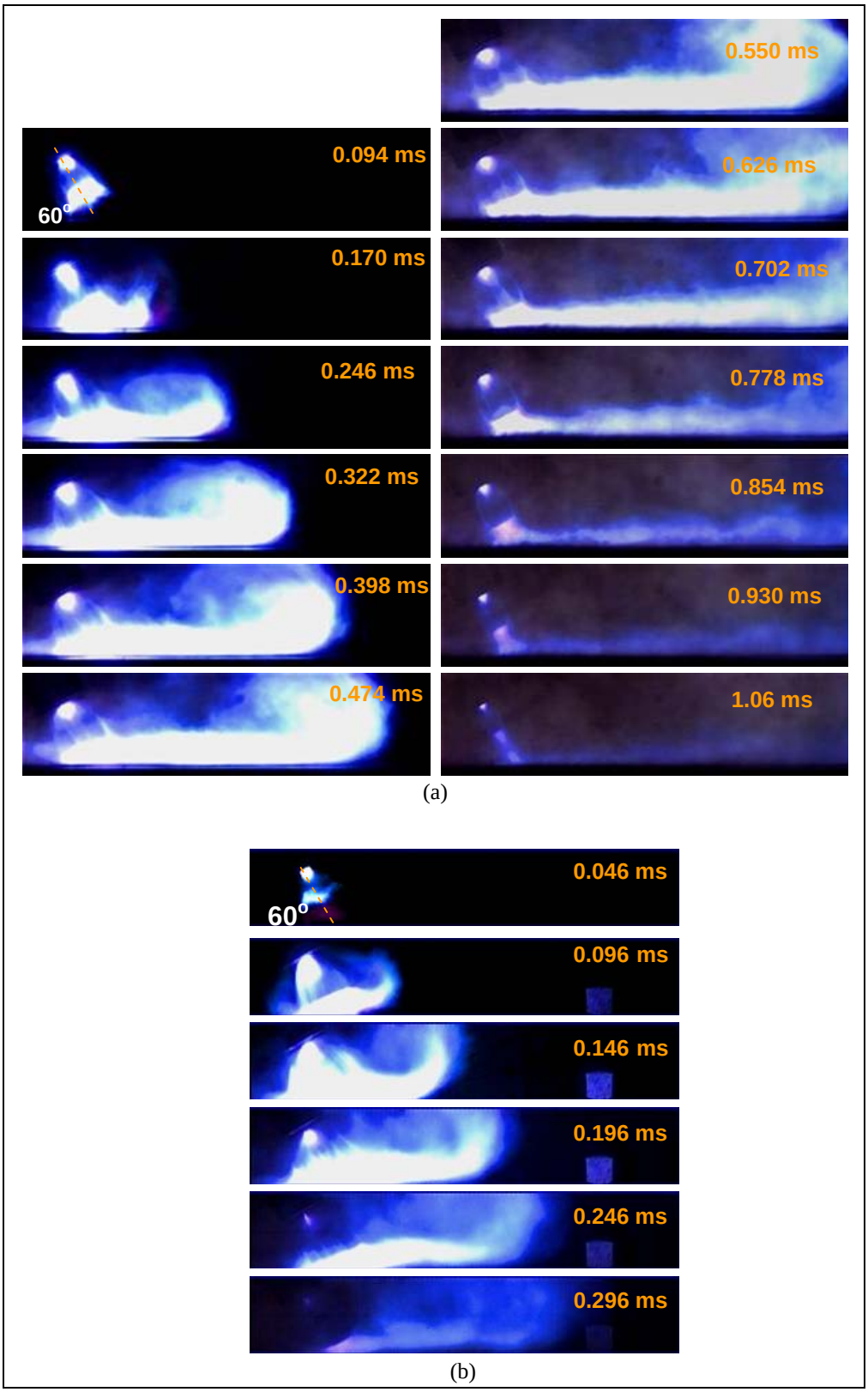

Figure 6. The 60° plasma jet impingement flows: (a) long pulse length and (b) short pulse length.

3.1.3 The 45° Impingements

As displayed in figure 7a, a fairly similar flow process occurred in the 45° impingement as in the 60° impingement for the long pulse length. A close examination, however, reveals differences in several areas. The flame front propagated faster and traveled a greater distance along the plate at 45°. Meanwhile, the thickness of the mainstream in the direction of the jet incidence increased. As expected, the flow in the direction opposite to the mainstream became noticeably less.

For the short pulse length, the resulting flow field shown in figure 7b is very similar to the one for the 60° impingement exhibited in figure 6b. The exception is that the flow traveled a greater distance on the plate.

3.1.4 Flame Propagation Speeds

Figure 8a shows a plot for locations of the visible plasma fronts along the impingement plate as measured from the photographic data. Note that in all cases the visible plasma propagated in a fairly linear fashion during the early flow period. Using these data, the early plasma front propagation speeds are estimated and plotted in figure 8b. The result shows that the visible plasma propagated faster for the short pulse length, and the speed increased with decreasing incident angle of the jet flow.

3.2 Pressure Distributions

3.2.1 The 90° Impingements

Figure 9 presents the pressure measurements on the flat plate for both the long and short pulse lengths, and gives the voltage measurement as a time reference. Difficulties were often encountered in the measurements because of the presence of magnetic fields and charged particles coupled with highly transient flow interactions with the impingement plate. The figure shows that the pressure rises at P_o and P_1 nearly at the same time. The pressures were expected to vary in accordance with the distance between the nozzle and the plate, as well as the power output from the capillary. Oscillations occurred along the entire pressure-time traces. It is unsure whether all of the oscillations existed physically or were induced electronically.

A comparison between the two plots in figure 9 (note that they are plotted in different vertical scales) reveals an earlier pressure rise and a higher peak pressure for the short pulse. This behavior is consistent with the data given in figure 10b—a shorter pulse length resulted in a higher flame propagation speed.

3.2.2 The 60° Impingements

At the 60° incidence, the overall pressure behavior shown in figure 11 is similar to that recorded in the 90° impingement.

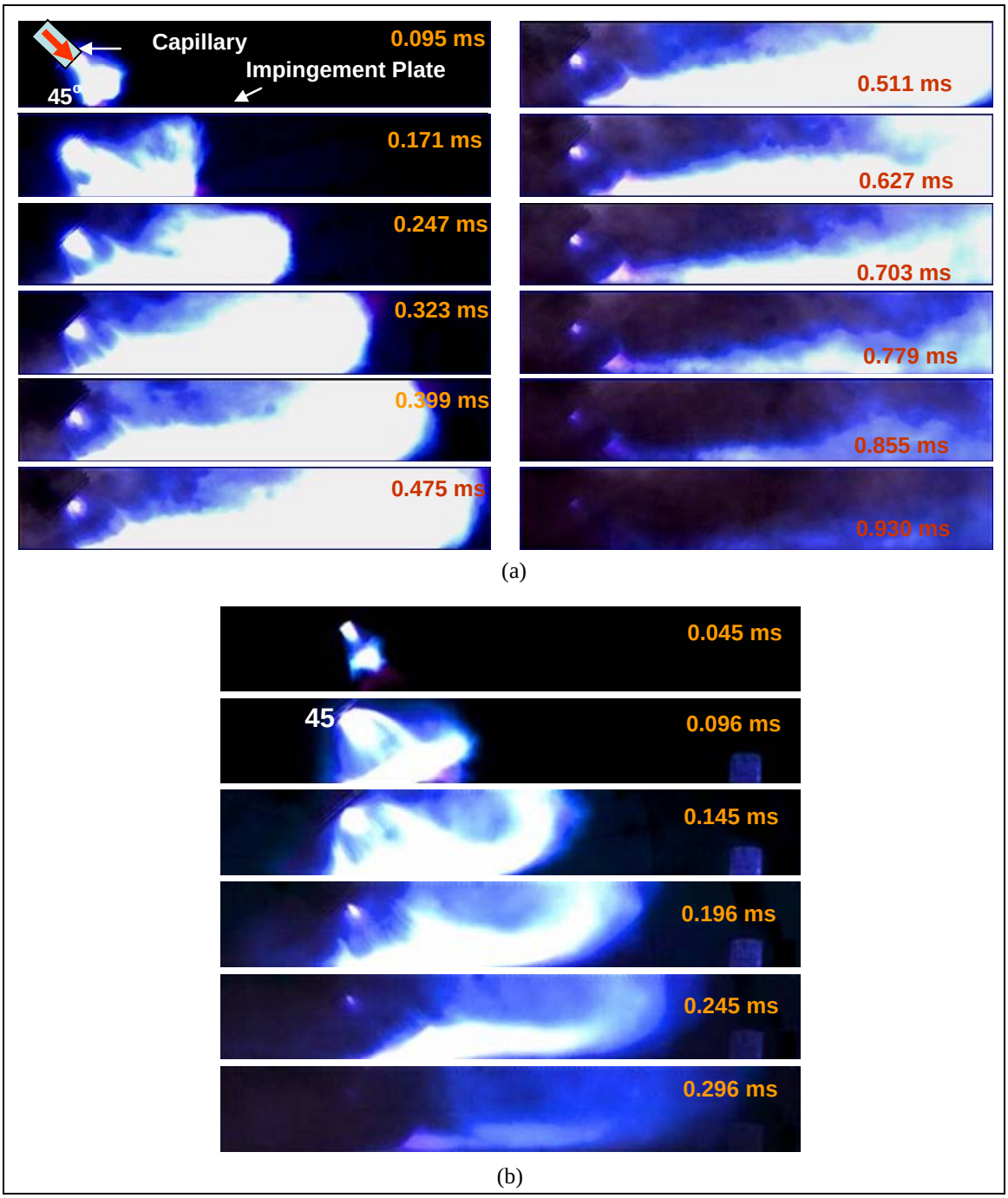

Figure 7. The 45° plasma jet impingement flows: (a) long pulse length and (b) short pulse length.

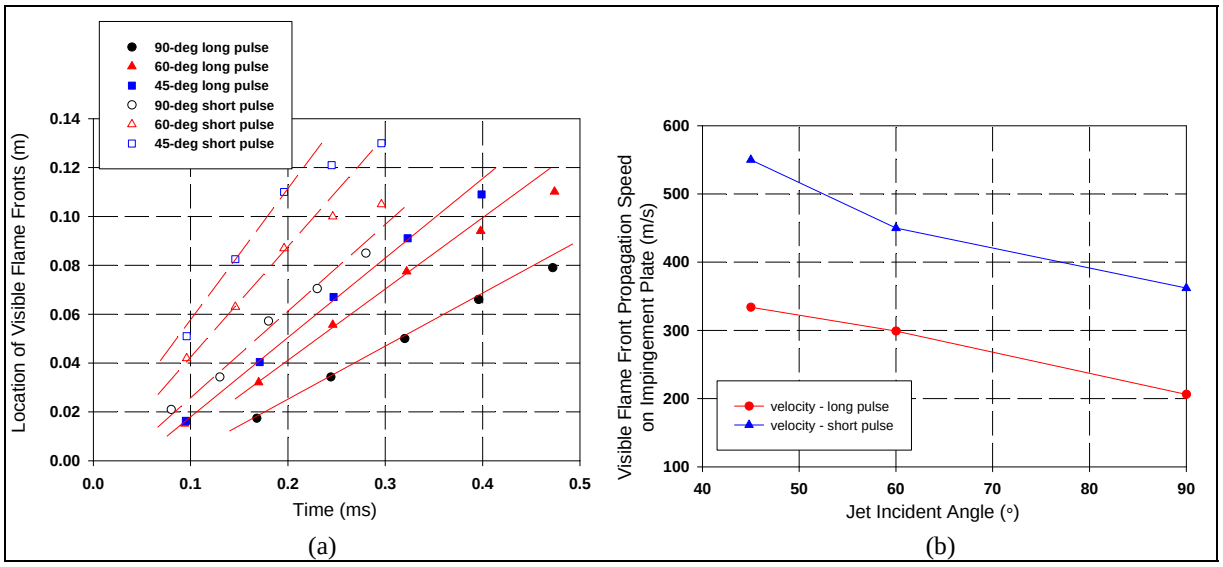

Figure 8. Plasma front spacial characteristics: (a) visible plasma front locations and (b) estimated propagation speeds.

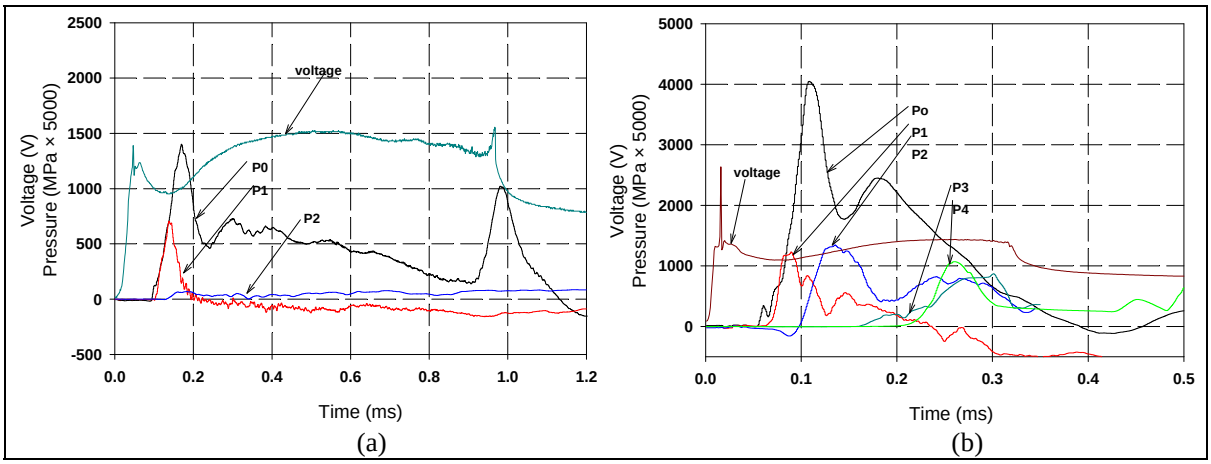

Figure 9. Pressure distributions for 90° impingement flows: (a) long pulse length and (b) short pulse length.

3.2.3 The 45° Impingements

At the 45° incidence, the overall time traces of the pressure given in figure 10 appear similar to those shown in figure 11. However, when the incidence angle is further reduced, say to 30°, a delay in the pressure rising times at locations farther from the stagnation region is expected to become more apparent.

Figure 10 also presents a set of pressure data measured in the lateral direction (i.e., perpendicular to the direction of the jet incidence). For the long pulse length, all pressure rises in the lateral direction occurred behind times measured in the direction of the jet incidence, implying a significant flow-speed drop in the lateral direction.

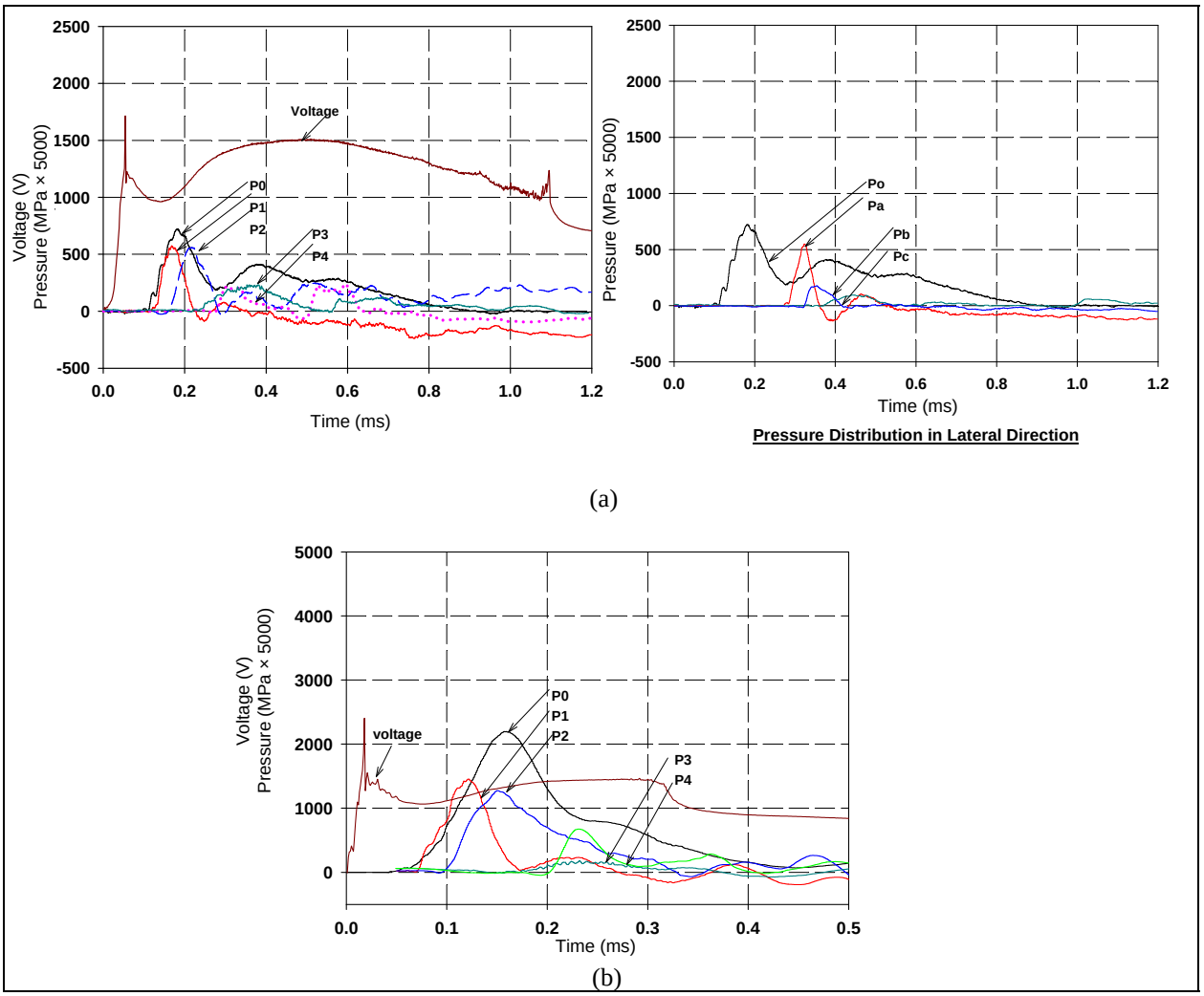

Figure 10. Pressure distributions for 45° impingement flows: (a) long pulse length and (b) short pulse length.

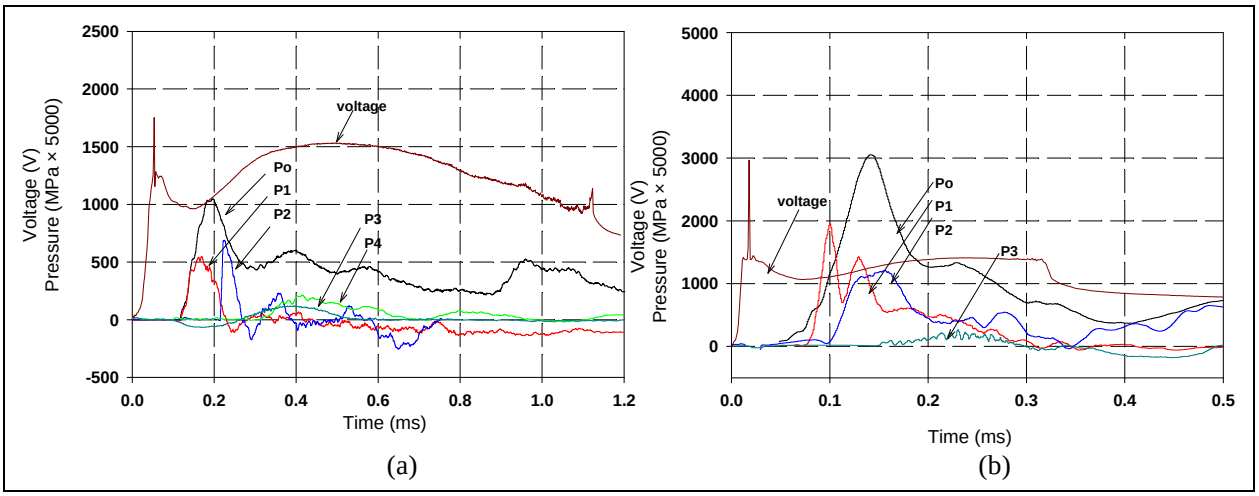

Figure 11. Pressure distribution for 60° impingement flows: (a) long pulse length and (b) short pulse length.

3.2.4 Comparison of Stagnation Pressures

When the pressure P_o of all tests are plotted together, figure 12 explicitly shows that the peak stagnation pressure was higher for the short pulse length and that the pressure decreased with a decreasing incident angle.

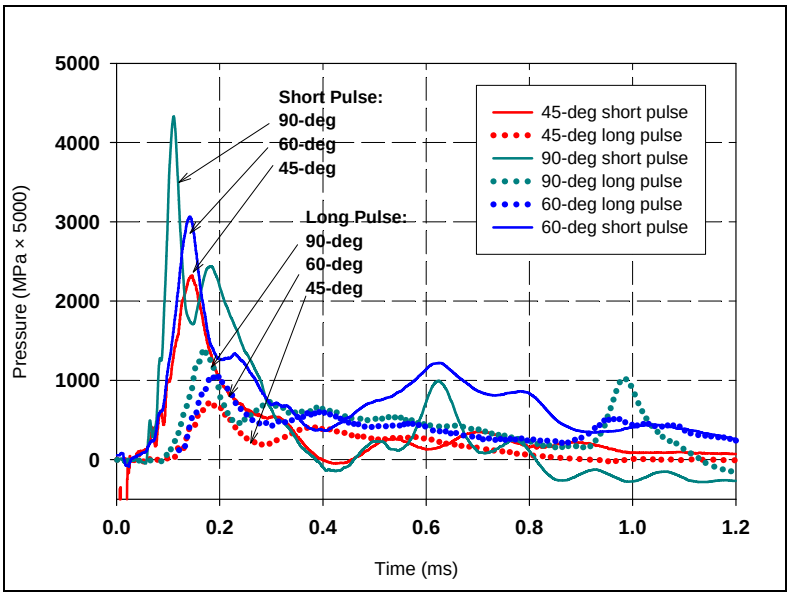

Figure 12. Stagnation pressure P_o for all tests.

3.3 Flow Signatures

Figure 13 exhibits traces of the high-speed flows on the impingement plate. Residue (fine particles) deposits produced from the erosion of the polyethylene tube in the capillary created the dark image. Numerous flow streaks in the radial direction are seen around the stagnation region. The nonuniformity of the streak-distribution appearance and the darkened area represents a nonuniform distribution of fine particles across the jet flow before arriving at the plate surface. There exists a bright (clean) area around the stagnation region, created by local high-speed flows. Furthermore, scorches found on the impingement plate were caused by the moving heavy particles produced from the exploding wire and the erosion of the steel nozzle's inner surface is through which the plasma was discharged. These particles could carry a certain amount of kinetic energy and heat to the impingement plate. Therefore, in an actual charge system, the particles could contribute significantly to the ignition stimulus required for the charge system.

The stagnation region for the long pulse length was much smaller in comparison, although the total flow-trace areas on the impingement plate were about the same. The shape of the flow signature varied with the incident angle (longer and narrower for a smaller incident angle).

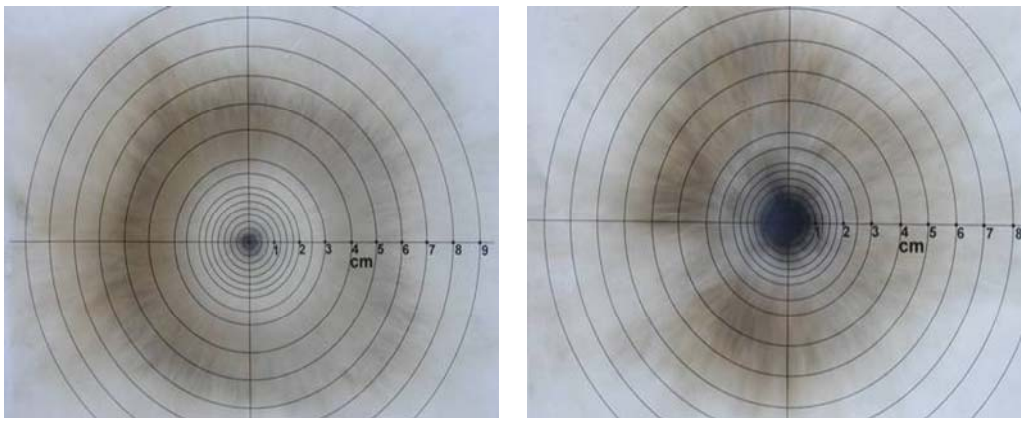

Pulse length = 1.0 ms Pulse length = 0.3 ms

(a)

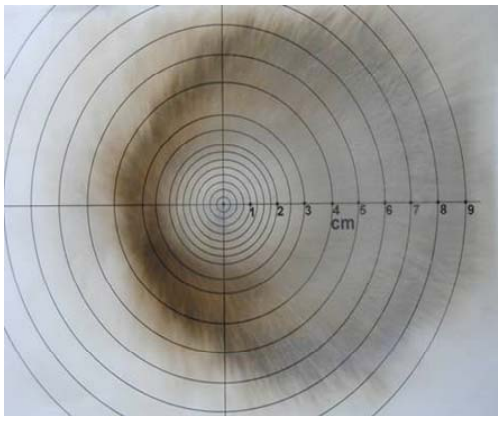

Pulse length = 1.0 ms

(b)

Figure 13. Flow signatures: (a) 90° impingement and (b) 45° impingement.

3.4 Light Intensity of Flow Fields

Measuring direct temperature of the flow or the surface of the impingement plate by thermocouples seems improbable in such a severe environment involving magnetic effects, shock wave interactions, and highly transient flows. The following simple measuring methods can be used to compare the thermal effect between the two pulse lengths of interest.

In this test series, a direct flow-field comparison was made in terms of the flow-field size and the brightness of the images obtained from the high-speed camera with an identical optical setting of framing rate, lens aperture, and filter. Figure 14 shows the results for two 90° impingement flows—one for the long pulse length and the other for the short pulse length. It is clear that for

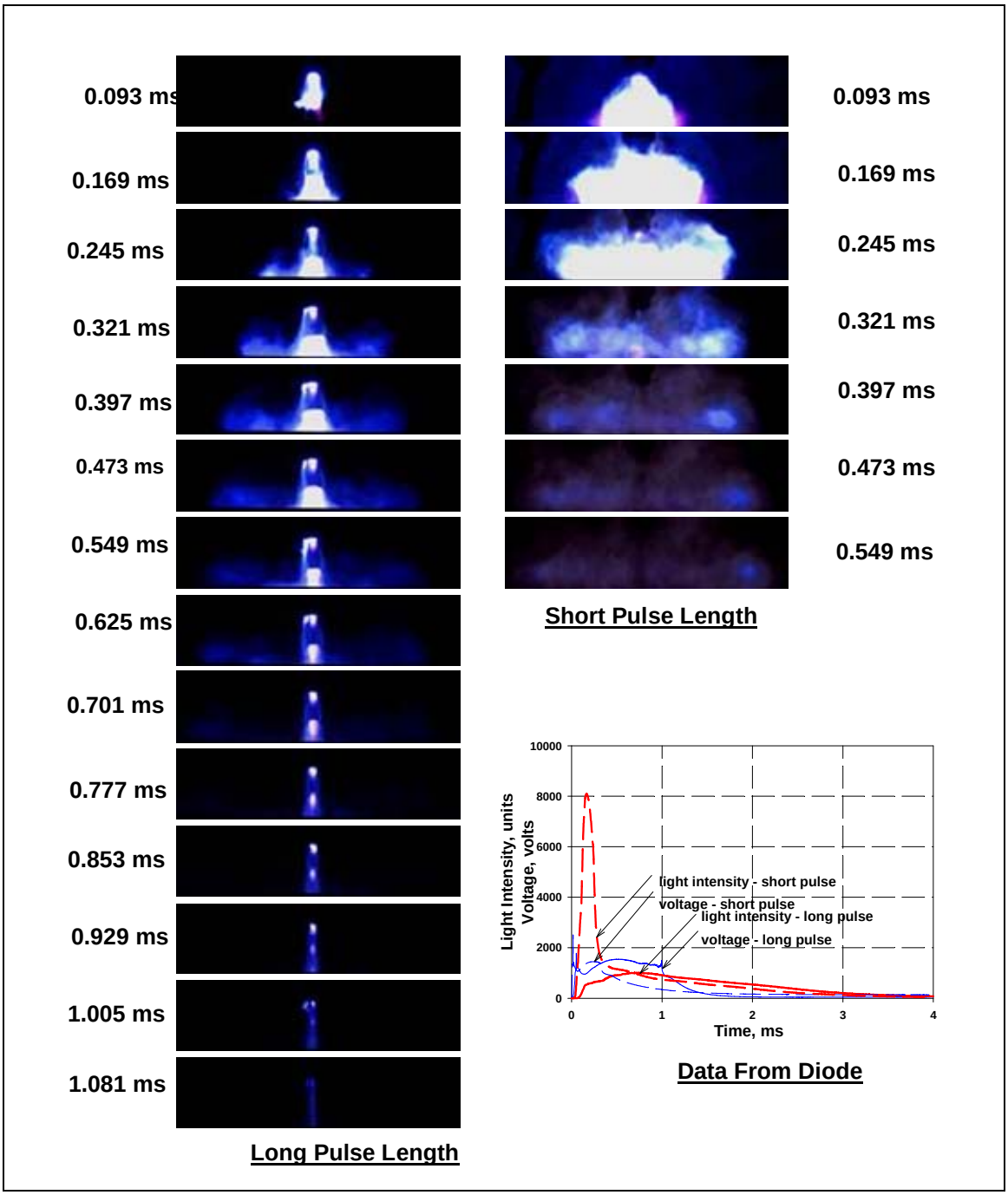

Figure 14. Light intensity comparison.

the short pulse length, the flow field was significantly larger and its light intensity was much higher. However, the time duration was reduced to one-third of the time duration of the long pulse length.

During the same tests, a photodiode, positioned 60 cm away from the stagnation region, was employed to monitor the light intensity of the flow field. The resulting plot shows that the maximum light intensity for the short pulse length was approximately 8× that for the long pulse length. Unlike the images from the camera showing that the visible light faded away at the end of the pulse length, the light intensity measured by the diode stayed for a few more milliseconds beyond the pulse length. This discrepancy could be due to the possibility that the diode used records data in a broader band of electromagnetic spectrum than the digital camera.

Since light emissions from the plasma interact with some propellants at a certain surface depth (*20*), stronger emissions resulting from a short pulse length could better promote fast ignition of a charge. On the other hand, a greater flow penetration into the propellant bed and a longer duration of flow interaction resulting from a longer pulse length could achieve a more effective ignition for propellants more easily ignited by convective heat transfer. The relative importance of these two effects has to be weighed in accordance with the propellant formulation and the charge configuration. Therefore, it is clear that the pulse length needs to be optimized in order to best fit a given propelling charge system.

4. Summary and Conclusion

In the present experiments, several interesting and important flow characteristics have been observed in both normal and oblique plasma jet impingements on a flat plate for two pulse lengths of approximately 0.3 and 1.0 ms. Result comparisons are made for the influence of the pulse length.

In all tests, the photographic and pressure data indicated that plasma jet impingement flows were highly transient and turbulent. A shorter pulse length would result in a wider flow field, faster flow process, higher light intensity, and shorter time duration of flow interaction. Additionally, the stagnation region on the impingement plate was larger, and the stagnation pressure was higher in comparison with those obtained from a longer pulse length.

The incident angle of a plasma jet impinging on a flat plate also plays an important role in influencing the flow characteristics. A smaller incident angle resulted in a lower stagnation pressure, but a higher flame propagation speed along the impingement plate. Additionally, it gave a longer, but narrower, flow coverage area on the impingement plate.

These experimental studies have elucidated many insights into the plasma jet flows and have shown that the plasma pulse length can have a strong influence on the flow characteristics (including radiation) and, consequently, on the plasma-propellant interactions. Therefore, the plasma pulse length should be optimized in order to achieve a highly effective ignition of a propulsion system with a minimum demand of electrical energy.

5. References

1. Perelmutter, L.; Sudai, M.; Goldenberg, C.; Kimhe, D.; Zeevi, Z.; Arie, S.; Melnik, M.; Melnik, D. Temperature Compensation by Controlled Ignition Power in SEPTC Guns. *Proceedings of the 16th International Symposium on Ballistics*, San Francisco, CA, 23–28 September 1996; pp 145–152.

2. Dyvik, J.; Katulka, G. L. ETC Temperature Compensation: Experimental Results of 120-mm Test Firings. *Proceedings of the 33rd JANNAF Combustion Meeting*, November 1996; CPIA Publication 653, Vol. III, pp 111–119.

3. Del Güercio, M. A. Propellant Burn Rate Modification by Plasma Injection. *Proceedings of the 34th JANNAF Combustion Meeting*, October 1997; CPIA Publication 662, Vol. I, pp 35–42.

4. Wren, G. P.; Oberle, W. F.; Hosangadi, A. Influence of Radiation on Grain Heating in ETC Closed Chambers. *IEEE Transactions on Magnetics* **1999**, *35* (1), 234–239.

5. White, K. J.; Katulka, G. L.; Khun, T.; Nekula, K. *Plasma Characterization for Electro-Thermal-Chemical (ETC) Gun Applications*; ARL-TR-1491; U.S. Army Research Laboratory: Aberdeen Proving Ground, MD, 1997.

6. Taylor, M. J.; Dunnett, J. A Description of the Wire Explosion Process for ETC Plasma Generators. *IEEE Transactions on Magnetics* **2003**, *39* (1), 269–274.

7. Nusca, M. J.; White, K. J.; Williams, A. W.; Landsberg, A. M.; Young, T. R.; Lind, C. A. Computational and Experimental Investigations of Open-Air Plasma Discharges, *37th Aerospace Science Meeting and Exhibit*, Reno, NV, 11–14 January 1999; AAIA Paper No. 99-0865.

8. Nusca, M. J.; McQuaid, M. J.; Anderson, W. R. *Multispecies Reacting Flow Model for the Plasma Efflux an ETC Igniter-Application to the Open-Air Plasma Jet Impinging on an Instrumented Plate*; ARL-TR-3275; U.S. Army Research Laboratory: Aberdeen Proving Ground, MD, 2004.

9. Taylor, M. J. Measurement of the Properties of Plasma from ETC Capillary Plasma Generators. *IEEE Transactions on Magnetics* **2001**, *37* (1), 194–198.

10. White, K. J.; Williams, A. W.; Nusca, M. J. Plasma Output and Propellant Radiation Absorption Characteristics. *Proceedings of the 35th JANNAF Combustion Meeting*, December 1998, CPIA Publication 680, Vol. I, pp 237–246.

11. Williams, A. W.; White, K. J. Plasma-Propellant Interaction Studies: Measurements of In-Depth Propellant Heating by Plasma Radiation; Investigation of Possible Plasma-Induced Propellant Erosion. *Proceedings of the 36th JANNAF Combustion Meeting*, October 1999; CPIA Publication 691, Vol. II, pp 67–76.

12. Kaste, P.; Kinkennon, A.; Lieb, R.; Birk, A.; Del Güercio, M.; Newberry, J.; Schroeder, M.; Pesce-Rodriguez, R. Surface Phenomena of Plasma-Treated Propellant Samples. *Proceedings of the 36th JANNAF Combustion Meeting*, October 1999; CPIA Publication 691, Vol. II, pp 67–76.

13. Nusca, M. J.; White, K. J. Plasma Radiative and Convective Interactions with Propellant Beds. *Proceedings of the 34th JANNAF Combustion Meeting*, October 1997; CPIA Publication 662, Vol. II, pp 21–33.

14. Fifer, R. A.; Sagan, E. S.; Beyer, R. A. Investigation of the Role of Plasma Chemistry in the Plasma Propellant Ignition (PPI) Process. *Proceedings of the 38th JANNAF Combustion Meeting*, April 2002; CPIA Publication 712, Vol. I, pp 259–268.

15. Li, J. Q.; Zhou, H.; Kudva, G.; Thynell, S.; Litzinger, T. Experimental Investigations of Plasma Propellant Interactions. *Proceedings of the 37th JANNAF Combustion Meeting*, November 2000; CPIA Publication 701, Vol. I, pp 109–121.

16. Chang, L. M.; Howard, S. L. Characterization of Plasma Jet Flows and Their Interaction With Propelling Charges. *Proceedings of 20th International Symposium on Ballistics*, Orlando, FL, 23–27 September 2002.

17. Chang, L. M.; Howard, S. L. *Narrow Channel Flame Propagation Characterization of Disc Propellant Charges with Plasma Ignition*; ARL-TR-3506; U.S. Army Research Laboratory: Aberdeen Proving Ground, MD, 2005.

18. Beyer, R. A.; Pesce-Rodriguez, R. A. Experiments to Define Plasma-Propellant Interactions. *IEEE Transactions on Magnetics* **2003**, *39* (1), 207–211.

19. Taylor, M. J. Consideration of the Energy Transfer Mechanisms Involved in SETC Ignition System. *IEEE Transactions on Magnetics* **2003**, *39* (1), 262–268.

20. Beyer A. R.; Pesce-Rodriguez, R. A. The Role of Radiation in Plasma-Propellant Interactions. *Proceedings of the 21st International Symposium on Ballistics*, Adelaide, Australia, 19–23 April 2004.

21. Li, J.; Litzinger, T. A.; Thynell, S. T. Interactions of Capillary Plasma with Double-base and Composite Propellants. *Journal of Propulsion and Power* **2004**, *20* (4), 675–683.

22. Das, M. S.; Thynell, S. T.; Li, J.; Lizinger, T. A. Material Dependence of the Transient Radiative Heat Transfer from a Plasma Produced by a Capillary Discharge. *Proceedings of the 40th JANNAF Combustion Meeting*, Charleston, SC, 13–17 June 2005.

23. Das, M. S.; Thynell, S. T.; Li, J.; Lizinger, T. A. Transient Radiative Heat Transfer from a Plasma Produced by a Capillary Discharge. *J. Thermophysics and Heat Transfer* **2005**, *19* (4), 572–580.

24. Chang, L. M.; Howard, S. L.; Beyer, R. A. Characterization of Plasma Jet Flows and Their Interaction with Propelling Charges. *Proceedings of the 20th International Symposium on Ballistics*, Orlando, FL, 23–27 September 2002.

25. Nusca, M. J.; Howard, S. L. *Experiment and Modeling Studies of Plasma Injection by an Electrothermal Igniter into a Solid Propellant Gun Charge*; ARL-TR-3806; U.S. Army Research Laboratory: Aberdeen Proving Ground, MD, 2006.

26. Chang, L. M.; Howard, S. L. *Electrothermal-Chemical Plasma Ignition of Gun-Propelling Charges: The Effect of Pulse Length*; ARL-TR-4253; U.S. Army Research Laboratory: Aberdeen Proving Ground, MD, 2007.

27. Beyer, R. A.; Brant, A. L. Plasma Ignition in a 30-mm Cannon. *IEEE Transactions on Magnetics* **2007**, *43* (1), 294–298.

NO. OF
COPIES ORGANIZATION

1 (PDF ONLY) DEFENSE TECHNICAL INFORMATION CTR
DTIC OCA
8725 JOHN J KINGMAN RD
STE 0944
FORT BELVOIR VA 22060-6218

1 US ARMY RSRCH DEV & ENGRG CMD
SYSTEMS OF SYSTEMS INTEGRATION
AMSRD SS T
6000 6TH ST STE 100
FORT BELVOIR VA 22060-5608

1 DIRECTOR
US ARMY RESEARCH LAB
IMNE ALC IMS
2800 POWDER MILL RD
ADELPHI MD 20783-1197

1 DIRECTOR
US ARMY RESEARCH LAB
AMSRD ARL CI OK TL
2800 POWDER MILL RD
ADELPHI MD 20783-1197

ABERDEEN PROVING GROUND

1 DIR USARL
AMSRD ARL CI OK TP (BLDG 4600)

NO. OF COPIES ORGANIZATION

2 COMMANDER
US ARMY ARDEC
AMSRD AAR AIS SE
W MILLER
BLDG 1
PICATINNY ARSENAL NJ
07806-5000

2 COMMANDER
ARO
TECH LIB
D MANN
PO BOX 12211
RESEARCH TRIANGLE PARK NC
27709-2211

1 COMMANDANT
US ARMY CMD & GEN
STAFF COLLEGE
FORT LEAVENWORTH KS 66027

1 DIRECTOR
US ARMY RESEARCH LAB
AMSRD ARL RO P
R SHAW
TECH LIB
PO BOX 12211
RESEARCH TRIANGLE PARK NC
27709-2211

1 COMMANDER
US ARMY ARDEC
TECH LIB
PICATINNY ARSENAL NJ 07806-5000

1 COMMANDER
NAVAL RSRCH LAB
TECH LIB
BLDG 59
WASHINGTON DC 20375-5000

1 OFFICE OF NAVAL RSRCH
J GOLDWASSER
875 N RANDOLPH ST RM 653
ARLINGTON VA 22203-1768

1 COMMANDER
NSWC
TECH LIB
INDIAN HEAD MD 20640-5000

NO. OF COPIES ORGANIZATION

1 COMMANDER
NSWC
TECH LIB
DAHLGREN VA 22448-5000

1 COMMANDER
NAWC
INFORMATION SCI DIV
CHINA LAKE CA 93555-6001

ABERDEEN PROVING GROUND

20 DIR USARL
AMSRD ARL WM BD
R BEYER
L M CHANG (3 CPS)
J COLBURN
P CONROY
A BRANT
S HOWARD (3 CPS)
M NUSCA
B FORCH
A WILLIAMS
R PESCE-RODRIGUEZ
P KASTE
J SCHMIDT
AMSRD ARL WM M
J BEATTY
B RINGERS
J SMITH
AMSRD ARL WM MC
R ADLER